

Physical Model of a Twin-scroll Turbine with Unsteady Flow

Author, co-author (Do NOT enter this information. It will be pulled from participant tab in MyTechZone)

Affiliation (Do NOT enter this information. It will be pulled from participant tab in MyTechZone)

Copyright © 2015 SAE International

Abstract

The paper describes a way to a 1-D central streamline model of a radial turbine flow, suitable for twin-scroll description and based on approximation of real physics of flow mixing and energy transformation. The original 1-D model of a single scroll turbine, described earlier in numerous SAE papers, has been amended by twin-scroll nozzles (both vaneless or with blade cascades) and mixing of individual partitions of flows upstream of additional vaneless nozzle and an impeller. This model is transferable to 1-D unsteady simulations as it is (i.e., using quasi-steady approach) or using 1-D unsteady solvers. It has suitable features even for more detailed description of turbine flows and energy transformation. The first results of pulse influence on turbine maps delivered expected results consisting of complicated interaction between individual losses.

The model itself is not fully predictive, using experimentally or in CFD found loss coefficients, but it is suitable for extrapolation of experience from similar systems before detailed CFD simulation or experiments are done. The new model can be used especially transferring turbine features found during mapping back to the design stage at a turbocharger manufacturer.

The features of twin scroll turbines call for appropriate optimization of turbines for high pulsation factor, as they are currently used for twin-scroll four cylinder engine turbochargers (two cylinders with 360° distance between pulses). The results of turbine matching should be used as a feed-back for turbine design.

Introduction

High low-end ICE torque of turbocharged and massively downsized engines calls for efficient boost pressure control, which causes issues especially at SI engines featuring high exhaust gas temperatures. There is a natural way of turbine self-control at low mass flow rates, consisting in the use of relative high pressure pulsations, if engine speed is reduced – [1]. It strengthened high-pulsation exhaust manifolds, which improve exhaust gas energy transfer especially while engine runs at reduced speed – [8]-[10]. The small volume of this manifolds and possible interference of pressure pulses between exhausting cylinders call for pulse manifolds with in-time separated exhaust periods. Therefore, manifolds divided into branches connected to multiple turbine inlets are used. In the case of radial turbine, mostly twin-scroll design is used in automotive applications, although even quad-entry turbines can be found in the medium-speed engine business. The experience with partial admission from axial turbines and from momentum mixing in pulse-converters is inspiring

– [6], [7], [40] and [41], but it calls for taking specific features of mixing in radial twin scroll into account.

The lack of turbine maps, if twin scroll or divided scroll is used for radial turbine stator entry, is well-known. Many attempts were done to find them from the measurements at a turbine steady-flow test bed in a suitable form for turbine matching by simulation. Recently, specific test facilities were built. Test results are available at turbine manufacturers, mostly as confidential data. Published results can be found, e.g., in [34], [36] or [39], especially for asymmetric turbine scrolls.

The nature of in-turbine processes at possibly separated boundary layers and blade tip leakages – [5], [11], Coriolis acceleration field [5] and transonic conditions [2] is rather complicated for direct and sufficiently fast 3-D simulation, since the needs for mesh density are extraordinary high. Therefore, simulation approaches offer wide range of models, based on 1-D or 3-D, e.g., [16] - [19], [23] – [26] or recently on [35], [36] and [38]. 3-D seems to be a solution for the future, but still it needs the same calibration as 1-D does. Moreover, the detailed geometry data are not usually released by turbocharger manufacturers. Time requirements of 3-D simulations are still rather far from optimization feasibility.

The physical modelling using experiments at a specific test bed with pulsating flow is useful for qualitative understanding, e.g., [12] – [15]. Since the gas at a test bed is often cold, and the pulses are not similar to working engine conditions, this method cannot yield final results for other engine sizes, especially if not associated with analysis of in-turbine phenomena. The combination of different depths of physics with experiments is needed [21] - [26] and dedicated experiments, as in [22] or [27], are worthwhile.

The attempts to respect the features of twin- or multiple-entry turbines are still on the half-way, if map-based model is to be used as a black-box. The measurements of detailed maps for twin-entry turbines are costly and time consuming, if different flow rates, pressure ratios or even temperatures at both entries should be respected during measurements – e.g. [34]. The interpolation in maps at simulated engine has to be done in iterative way, since the turbine mass flow rate capacity depends not only on a pressure ratio in a simulated branch but also on the mass-flow rate in the other partition. Moreover, any lookup-map based on interpolation suffers from lack of physical fundamentals, since the mixing processes take place inside a turbine at governing pressure differences significantly different from turbine inlet pressures, used, e.g., in [39]. Using of a turbine model, composed of two (nearly) independent turbines with the same speed, has to be amended by a virtual cross-link between

partitions to take the other partition pressure waves into account. Even in this case, the pressures governing a mixing process are not respected well and the orifice area has to be calibrated – [28].

In the past, several models were developed for simulation of unsteady 1-D flow in a radial turbine including the influence of centrifugal force in an impeller – e.g., [3], [9] or [16]. The current state-of-the-art offers well-proven 1-D solvers, sufficiently opened for the purposes intended by this task – e.g. [29]. There is no need to re-develop them, especially if they are integrated to the whole engine and powertrain model. This procedure is based on experience with similar approach to pressure-wave supercharger or Roots blower modelling applied to larger system – [32] or [33].

This situation yielded the motivation for the current research, amending the results described in [23] – [26]. The well-proven system of unconventional use of already developed 1-D modules with control capabilities was applied, as described, e.g., in [26] or [29]. The use of 1-D solver modules is easier, if the solver contains boundary conditions with momentum mixing, as in flow splits of GT Power [28].

Turbine Physical-Based Model

Turbine impeller and leakages are modelled according to principles described in [23] and applied to 1-D solver in [24] – [26] but amended by a twin scroll entry, e.g., Figure 1.

The model is aimed at

- generating steady flow, twin-scroll turbine map for comparison and possible calibration by steady-flow experiments at a turbine test bed; unlike in the current systems, no interpolation between partial admission maps is needed;
- using calibrated inputs for external procedure to 1-D pressure waves simulating codes as a boundary condition with lumped parameters at the end of exhaust manifold branches, linking them with the adjacent common low-pressure exhaust pipe; in this case, the model is able to yield fast acting iterative procedure; the results are mass flow rates in both branches in dependence on pressures immediately upstream of turbine inlets and downstream of turbine outlet; the side effects are simulation of both instantaneous efficiency and power of a turbine;
- being described directly by modules of 1-D solver, like GT Power; it enables the user respecting of pressure waves inside a turbine system, as used for single scroll turbine in [25] – [26].

There are other layouts of parallel multiple entry turbines, which can be transformed to this model, e.g., vaneless nozzles followed by a mixing zone or by a combination of mixing zone and additional bladed nozzle. Any vaneless nozzle is equivalent to a bladed one after calibration of exit angle, which is in this case pressure dependent, nevertheless. The standard assumption that the flow keeps its angle from a radius (the result of angular momentum and mass conservation) is correct only if density does not change too much, i.e., not close to Mach number equal to one.

Other solutions, using serial twin-entry scrolls (one scroll for an angle of $360^\circ/\text{number of scrolls}$) may be described using the same principles, although in a different way considering angle of attack at

the impeller. The difference between parallel and serial partitions connection is in mixing of both partition flows: in the former case, the mixing takes part mostly upstream of an impeller, in the latter one mixing proceeds in an impeller. The position of mixing area is thus used to distinguish between both cases.

In the most frequently used case, a twin scroll consists of inlet pipes followed by two nozzle-formed vertexes. In reality, they are vaneless or with blades, in general adjustable ones. At the end of inner wall and after partial expansion reducing both pressures in a scroll partitions, mixing of both flows is realized by a joint of both pipes. Another nozzle may follow, in reality could be vaneless or bladed again. After it, the standard model of an impeller and leakages, described in [23] and applied to 1-D in [26], is used.

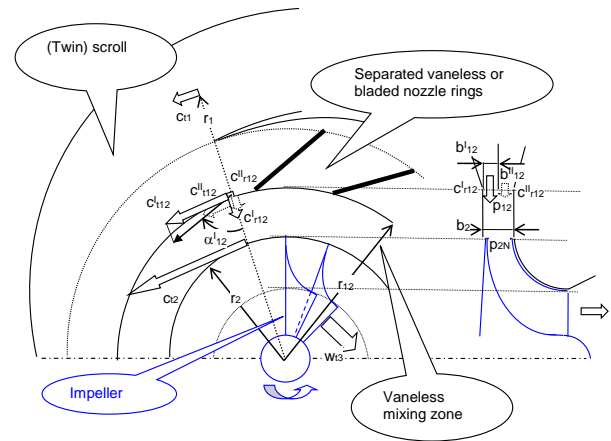


Figure 1. A scheme of parallel twin entry scroll with bladed nozzles and a vaneless mixing zone.

For this layout, a simplified algebraic model assuming steady flow has been developed together with 1-D unsteady model, using modules and modified solvers from GT Suite.

Algebraic Center-Streamline Model of a Twin-Scroll Radial Turbine

Although the basic equations are the same as described in [26], the structure of the model is completely different, which allowed for implementation of a mixing zone and fast iterative solution. The equations are solved for both mass flow-rates at entries as independent variables together with known stagnation temperatures at inlets and static pressure at a turbine impeller outlet.

The solution starts at turbine outlet and proceeds in a counter-flow direction upwind. The Newton-Gauss method, combined with additional iterations for loss coefficients, is used for finding static and stagnation pressures and temperatures in upwind direction. It is not possible without iterations, of course, since at least inlet stagnation temperatures have to be kept at fixed values. The outlet temperature has to be estimated to start upstream calculations. It is corrected at the end of procedure to inlet temperatures. Inlet stagnation pressures are the direct output of the numerical procedure. If fixed pressure ratio maps have to be found (unlike the case of standard turbine map measurement), another iteration to keep pressure ratio fixed is needed.

The backward going iteration is based on impeller total enthalpy conservation (including potential energy in the field of centrifugal force, so called rothalpy). Constant pressure thermal capacity is assumed to be independent of small temperature differences, therefore, reference temperature for zero enthalpy does not occur in the energy conservation equation. Now, leakage along impeller blades is assumed (all leakage flow leaves the impeller blades upstream of an interblade channel). Then, using known mass flow-rate and state downstream of impeller, energy conservation yields

$$\begin{aligned} c_p T_{2l} + \frac{w_2^2}{2} - \frac{u_2^2}{2} &= c_p T_3 + \frac{w_3^2}{2} - \frac{u_3^2}{2} \\ c_p T_3 \left(\frac{T_{2l}}{T_3} \right) + \frac{1}{2} \left(\frac{\dot{m}_l}{A_{2l} \rho_3} \right)^2 \left(\frac{\rho_3}{\rho_{2l}} \right)^2 &= c_p T_3 + \frac{1}{2} \left(\frac{\dot{m}_l}{A_{3l} \rho_3} \right)^2 - \frac{u_3^2 - u_2^2}{2} \\ c_p T_3 k_T \left(\frac{p_{2l}}{p_3} \right)^{\frac{\kappa-1}{\kappa}} + \frac{1}{2} \left(\frac{\dot{m}_l}{A_{2l} \rho_3} \right)^2 k_p \left(\frac{p_3}{p_{2l}} \right)^{\frac{2}{\kappa}} &= c_p T_3 + \frac{1}{2} \left(\frac{\dot{m}_l}{A_{3l} \rho_3} \right)^2 - \frac{u_3^2 - u_2^2}{2} = P \quad (1) \\ c_p T_3 k_T x^{\frac{\kappa-1}{\kappa}} + \frac{1}{2} \left(\frac{\dot{m}_l}{A_{2l} \rho_3} \right)^2 k_p x^{\frac{2}{\kappa}} - P &= 0 \end{aligned}$$

The last equation may be solved using Newton's method for unknown static pressure ratio:

$$\begin{aligned} c_p T_3 k_T \left(\frac{p_{2l}}{p_3} \right)^{\frac{\kappa-1}{\kappa}} + \frac{1}{2} \left(\frac{\dot{m}_l}{A_{2l} \rho_3} \right)^2 k_p \left(\frac{p_3}{p_{2l}} \right)^{\frac{2}{\kappa}} &= P \\ y = K_1 x^{\frac{\kappa-1}{\kappa}} + K_2 x^{-\frac{2}{\kappa}} - P & \\ \frac{dy}{dx} = \frac{\kappa-1}{\kappa} K_1 x^{\frac{1}{\kappa}} - \frac{2}{\kappa} K_2 x^{-\frac{2+\kappa}{\kappa}} & \quad (2) \\ x_{i+1} = x_i - \frac{y_i}{\left(\frac{dy}{dx} \right)_i} & \end{aligned}$$

The yet unknown correction coefficients have to be iterated since for the sake of simplicity they are not included into derivative. It is possible, but since the iteration converges fast, it is not needed to do it in a separate loop. Moreover, as described below, there are other inevitable needs for iteration loops combined with basic Newton procedure. Using the definition of expansion efficiency and relations between stagnation or total and static states, the correction by multiplier may be applied.

$$\begin{aligned} \eta_l &= \frac{\frac{w_3^2}{2}}{T_{rel02l} \left[1 - \left(\frac{p_3}{p_{rel02l}} \right)^{\frac{\kappa-1}{\kappa}} \right]} ; \quad \frac{T_0}{T} = \left(\frac{p_0}{p} \right)^{\frac{\kappa-1}{\kappa}} \\ k_T &= \frac{\frac{T_{2l}}{T_3}}{\left(\frac{p_{2l}}{p_3} \right)^{\frac{\kappa-1}{\kappa}}} = \frac{\frac{T_{2l}}{T_{rel02l}} \cdot \frac{T_{rel02l}}{T_3}}{\left(\frac{p_{2l}}{p_3} \right)^{\frac{\kappa-1}{\kappa}}} = \frac{\left(\frac{p_3}{p_{rel02l}} \right)^{\frac{\kappa-1}{\kappa}}}{1 - \eta_l \left[1 - \left(\frac{p_3}{p_{rel02l}} \right)^{\frac{\kappa-1}{\kappa}} \right]} = \frac{\left(\frac{p_3}{p_{2l}} \right)^{\frac{\kappa-1}{\kappa}}}{1 - \eta_l \left[1 - \left(\frac{p_3}{p_{2l}} \right)^{\frac{\kappa-1}{\kappa}} \right]} \quad (3) \\ \frac{\rho_3}{\rho_{2l}} &= \left(\frac{p_3}{p_{2l}} \right)^{\frac{1}{\kappa}} \frac{1}{k_T} \quad k_p = \left(\frac{1}{k_T} \right)^2 \end{aligned}$$

Taking into account that relative velocity at inlet to the interblade channel for a standard impeller is radial one and outlet velocity is defined by average angle of blades, the cross-section areas with a

normal parallel to average flow direction corrected to blade thickness obstruction are found from the basic turbine geometry.

Using this backward going procedure, all velocities and relative stagnation state variables can be simply found now at impeller inlet (i.e., after incidence loss took part). The basic assumption for parallel scroll partitions calls for a complete flow mixing upstream of impeller. Unlike in existing models, in which energy conservation, i.e. mixing of enthalpies is taken into account – [35] or [38], the momentum exchange creates fundamental part of the physically based model as described below. Otherwise the losses of kinetic energy, which are typical for any mixing with momentum conservation, can be respected in appropriate way by changes of discharge coefficients in dependence on mass flow rate ratios, which calls for additional iterations. The incidence loss reference velocity needs not to be approximated. Nevertheless, other iteration is needed since the relative tangential velocity before incidence loss takes part has to be found. That is why the following procedure starts with scroll outlets mixing. The individual mass flow rates and stagnation temperatures at scroll partition inlets are assumed to be fixed (and mutually different in general). The following relations without superscripts are applied for both scroll partitions – [23]

$$\begin{aligned} \left(\dot{m}^I + \dot{m}^II \right) c_p T_{02N} &= \left[\dot{m}^I c_p T_{01}^I + \dot{m}^II c_p T_{01}^{II} \right] \\ T_{02N} &= \frac{\dot{m}^I T_{01}^I + \dot{m}^II T_{01}^{II}}{\dot{m}^I + \dot{m}^II} \quad (4) \end{aligned}$$

The scroll partitions outlet velocities can be found if static outlet pressure is known. Let's assume it for a moment.

$$\begin{aligned} c_{2N}^I &= \frac{\dot{m}^I}{A_{2N}^I \frac{p_{2N}}{r T_{2N}^I}} ; \quad c_p T_{01}^I = c_p T_{2N}^I + \frac{c_{2N}^{I2}}{2} \\ \frac{1}{2} \left(\frac{r \dot{m}^I}{A_{2N}^I p_{2N}} \right)^2 T_{2N}^{I2} + c_p T_{2N}^I - c_p T_{01}^I &= 0 ; \quad T_{2N} = \frac{-c_p + \sqrt{c_p^2 + 2c_p T_{01} \left(\frac{r \dot{m}}{A_{2N} p_{2N}} \right)^2}}{\left(\frac{r \dot{m}_N}{A_{2N} p_{2N}} \right)^2} \quad (5) \end{aligned}$$

Now partition outlet velocities and both tangential and radial components (using known exit angles) can be found.

If immediate mixing is assumed at radius of scroll partitions outlet with no pressure change (it can be corrected by calibration coefficient K_m), the momentum conservation yields – [23]

$$\begin{aligned} c_{r2N} &= \left(\frac{\dot{m}^I}{\dot{m}^I + \dot{m}^II} c_{r2N}^I + \frac{\dot{m}^II}{\dot{m}^I + \dot{m}^II} c_{r2N}^{II} \right) K_m = w_{r2N} \\ c_{t2N} &= \frac{\dot{m}^I}{\dot{m}^I + \dot{m}^II} c_{r2N}^I \tan \alpha_2^I + \frac{\dot{m}^II}{\dot{m}^I + \dot{m}^II} c_{r2N}^{II} \tan \alpha_2^{II} \quad (6) \end{aligned}$$

These equations complicate the iterations substantially but they are fundamental for appropriate modelling of physics of losses inside at twin-scroll turbine. Since momentum flux depends on mass flow rate and velocity itself, it is dependent on velocity squared as kinetic energy is. The common velocity of mixed flow means, nevertheless, that kinetic energy is dissipated by mixing (as it is in the case of impact of plastic bodies). The exact mixing model has to take into

account the velocities after expansion in twin scroll, i.e., it cannot be applied if detailed model of expansion in turbine is taken into account. This is the basic difference between recently published, lumped parameter models (except for [36] and the current model, having been developed since 2002 – [23]-[27]).

The described model can be simply changed for the case with a wall splitter of scrolls elongated up to impeller inlet. In such case, individual angles of attack to impeller vanes are respected for both partial flows and momentum mixing equation takes into account radial velocity components only (similar to the first equation of (6)).

Using known velocity components, the incidence angle relative to impeller blades can be found. The difference between radial relative velocity in impeller before and after the incidence loss can be respected by changing radial velocity (due to density difference and possible area reduction) without any change of relative tangential one:

$$\zeta_{I,inc} = 2 \frac{P_{rel02N} - P_{rel02I}}{\rho_{2I} w_{2I}^2} = (\tan \beta_2 + K_{imp})^2 = \left(\tan \alpha_{2I} - \frac{u_2}{w_{2I}} + K_{imp} \right)^2 = \left(\frac{c_{t2N} - u_2}{w_{2I}} + K_{imp} \right)^2 \quad (7)$$

Then knowing relative stagnation pressure at impeller inlet after incidence loss, the previous relation yields

$$P_{rel02N} = P_{rel02I} + \zeta_{I,inc} \rho_{2I} w_{2I}^2 \quad (8)$$

Static pressure and temperature at relative flow for impeller before incidence loss occurs can be found from standard, well-known relations.

Knowing the state parameters in the gap between a nozzle ring and an impeller, leakages at both shroud side and the impeller disk (hub side) may be found. Without these flows, the calibration of model may be impossible since the kinetic energy losses influence both flow-rates and efficiency in one direction (high losses – low flow-rate and poor efficiency), while leakage increases flow-rate with simultaneous reduction of efficiency.

$$\dot{m}_I = \dot{m}^I + \dot{m}^{II} - \Delta \dot{m}_{leakage} \quad (9)$$

As a result, we have now two relations for T_{2N} , namely the basic static and stagnation temperatures and (5). However, the latter one was deduced with assumption of exducer exit temperature T_3 . The difference between those results has to be used for correction of T_3 . This creates the last iteration, improved by numerical Newton method approximation.

At the end of the whole cycle, the definition of expansion efficiency is used for finding total pressure at partition inlet from pressure at partition outlet

$$\eta_N = \frac{\frac{c_{2N}^2}{2}}{T_{01} \left[1 - \left(\frac{P_{2N}}{P_{01}} \right)^{\frac{\kappa-1}{\kappa}} \right]} ; \quad P_{01} = \frac{P_{2N}}{\left(1 + \frac{c_{2N}^2}{2\eta_N T_{01}} \right)^{\frac{\kappa}{\kappa-1}}} \quad (10)$$

The additional nozzle between joining of both scroll partitions and an impeller is added in a similar way as described for this basic model.

Before the turbine power is calculated, windage losses of an impeller should be deduced from the total head obtained in expansion.

Then, turbine power can be found from mass flow-rate and specific power, usually from the equations of Stodola (difference of total enthalpies) or Euler (angular momentum conservation) using parameters at impeller inlet and exit in absolute (i.e., fixed in space) coordinate system – [26].

The outlined procedure is being completed by the treatment of possible transonic flows, limiting the velocities to sonic ones and changing accordingly pressure ratios, and by the backflow conditions for very high centrifugal forces in comparison to pressures available. No issues occurred during the preparation of those adjustments. In the case of backflow, the mixing equations are simplified since there is only single flow entering the turbine and flow splitting occurs instead of flow joining. The momentum mixing is replaced by conservation and the common pressure in the node of flow split. The losses for a backflow are calibrated by a backflow discharge coefficient.

The described model can be implemented into GT Power as an external procedure or it can be used separately for evaluation of experiments, finding calibration coefficients and prediction of twin-scroll turbine maps.

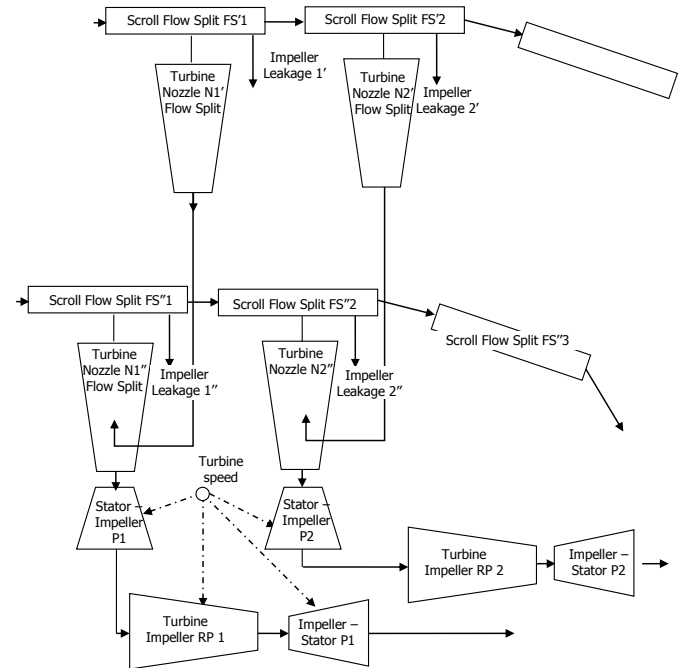


Figure 2. General unsteady model of a parallel twin scroll turbine with basic modules transferable to 1-D solver.

1-D Unsteady Flow Model of a Twin-Scroll Radial Turbine

As mentioned earlier, the modules of 1-D code were used in a specific structure with additional control elements to simulate details of flow in different parts of a system similar to the one shown in Figure 1.

The scheme of transformation of the model according to [26] into 1-D model is presented in Figure 2. Both scroll partitions may be divided into interconnected pipe or flow split modules and the outlet flows are subjected to mixing in the following flow splits or – better – joints. In currently available model, the serial splitting of a scroll partitions is significantly reduced. The model uses only one pipe and flow split per partition (i.e., no FS2, 3, etc.) and one pipe for impeller with external acceleration RP. The mixing in a turbine nozzle flow split takes part upstream of an impeller, as used in N1'-N1''. The layout, in this case transferred to GT Suite modules, is presented in Appendix, Figure 22.

The rest of the model, starting with Stator-Impeller stagnation state transformation P1, is the same as being referred to above, i.e., using transformation of stagnation states from steady coordinate system to rotating one, done in a specific orifice module with virtual heat transfer to change stagnation enthalpy appropriately (respecting impeller speed and inlet/outlet velocity triangles) and in a 1-D pipe RP1 – Figure 2 – under influence of centrifugal acceleration in dependence on impeller speed. The effective areas of connecting orifices are controlled according to the calibration data, listed in look-up tables or regression functions.

The turbine torque is integrated along a center streamline from local angular momentum changes, as described in details in [26]. Other – energy based – methods are not so simply applicable since the local drop of enthalpy and local mass flow rate has to be respected due to accumulation of mass and energy inside a turbine during unsteady flow operation.

Prediction of Turbine Maps

It should be stressed that the maps shown here are used in this case to demonstrate the changed turbine features and thus contribute to better understanding of the complicated matter only, not to define the turbine features for 1-D solver, as, e.g., GT Power and interpolate between them. That is why the presented model offers capability of direct simulation inside a 1-D engine simulation model without interpolating between prepared maps. The map prediction is important for model calibration, using the results from a turbocharger test bed, which is done by optimization code, as described in [24].

The 1-D solver input is in the case of 1-D modelling based on detailed modular model, which adds the power delivered by sections in appropriate physically accurate location, not at upstream of the turbine using inappropriate pressures or enthalpy heads.

Definition of a Twin-Scroll Turbine Parameters

Before the results are presented, the definitions of turbine map parameters have to be stated since it is not unambiguous, especially considering in reality non-existing perfect turbine state.

Enthalpy Head at a Turbine

Enthalpy head enables the calculation of turbine power. It is possible to use the Euler equation or a total enthalpy head. Then the usable enthalpy head and turbine power are obviously for a single scroll turbine:

$$\begin{aligned}\pi_T &= \frac{p_{01}}{p_3}; \quad c_s = \sqrt{2c_p T_{01} \left(1 - \pi_T^{\frac{1-\kappa}{\kappa}}\right)}; \quad BSR = \frac{u_2}{c_s} \\ c_T &= \sqrt{2\Delta h_T} = \sqrt{2(u_2 c_{t2N} - u_3 c_{t3} - \Delta h_{vent}) \frac{\dot{m}_I}{\dot{m}_N}} \\ P_T &= \dot{m}_N \frac{c_T^2}{2} \\ \eta_{Ts} &= \frac{c_T^2}{c_s^2}\end{aligned}\tag{11}$$

A reduction to leakage influence is involved. An ideal expansion velocity c_s and - for comparison - the apparent one c_T provide information for the isentropic efficiency and the blade tip velocity ratio **BSR**.

If a twin-scroll is used, the real turbine parameters are changed in an expected way

$$\begin{aligned}c_T &= \sqrt{2\Delta h_T} = \sqrt{2(u_2 c_{t2N} - u_3 c_{t3} - \Delta h_{vent}) \frac{\dot{m}_I}{\dot{m}^I + \dot{m}^{II}}} \\ P_T &= \left(\dot{m}^I + \dot{m}^{II} \right) \frac{c_T^2}{2}\end{aligned}\tag{12}$$

The issue is created by parameters of ideal turbine since they do not exist and have to be defined. Enthalpy head can be averaged using weighting by mass flow rate in a very natural way.

$$\begin{aligned}\pi_T^i &= \frac{p_{01}^i}{p_3}; \quad c_s^i = \sqrt{2c_p T_{01}^i \left(1 - \pi_T^{i\frac{1-\kappa}{\kappa}}\right)}; \quad BSR^i = \frac{u_2}{c_s^i} \\ c_s &= \sqrt{\frac{c_s^{I2} \dot{m}^I + c_s^{II2} \dot{m}^{II}}{\dot{m}^I + \dot{m}^{II}}}\end{aligned}\tag{13}$$

There is no simple procedure for averaging of pressure ratio. Approximately it can be weighted by mass flow-rate, as well, since the pressure difference creates the significant part of enthalpy head

$$\pi_T \approx \frac{\pi_T^I \dot{m}^I + \pi_T^{II} \dot{m}^{II}}{\dot{m}^I + \dot{m}^{II}}\tag{14}$$

More physically accurate procedure is averaging according to the enthalpy head, mass flow rate and total inlet temperature after mixing, i.e.,

$$2c_p T_{02} \left(1 - \pi_T^{\frac{1-\kappa}{\kappa}} \right) \left(\dot{m}^I + \dot{m}^{II} \right) = c_s'^2 \dot{m}^I + c_s''^2 \dot{m}^{II} \quad (15)$$

$$\pi_T = \left(1 - \frac{c_s'^2 \dot{m}^I + c_s''^2 \dot{m}^{II}}{2c_p T_{02} (\dot{m}^I + \dot{m}^{II})} \right)^{\frac{\kappa}{1-\kappa}}$$

The numerical exercise shows that both averaging methods are not very different, the difference not exceeding 5%. For the mass flow rate averaged pressure ratio, Saint-Venant-Wantzel equation is not directly suitable, since it cannot be solved for pressure ratio in closed form. The approximation was done using (15). Then, averaged discharge coefficient for the whole turbine is defined, if Saint-Venant-Wantzel relation is applied for the ideal case without losses

$$\mu_T = \frac{\dot{m}^I + \dot{m}^{II}}{m_{\text{Saint-Venant}}(\pi_T)} \quad (16)$$

Examples of Maps for Twin-Scroll Turbines with Partial Admission

The examples of dimensionless maps for a small turbine, used later in a 3.05 dm³ engine (Table 1) are presented in Figure 3 (turbine discharge ratio at low area rack position 0 with fixed turbine reference area for rack = 1, therefore low values of discharge coefficient) or Figure 4 (turbine total-to-static isentropic efficiency). The results were calculated using virtual turbine model based on GT Power modules - Figure 2 – coupled to a steady flow turbine test-rig simulated as well in GT Power. Fixed pressure ratio with different pressure differences between scroll partitions was defined for a virtual turbine inlet, namely uniform distribution without partial admission and pressure differences between branches 1.5 bar, keeping averaged pressure ratio fixed. The model of a single scroll was compared to twin scroll uniform admission case, as well.

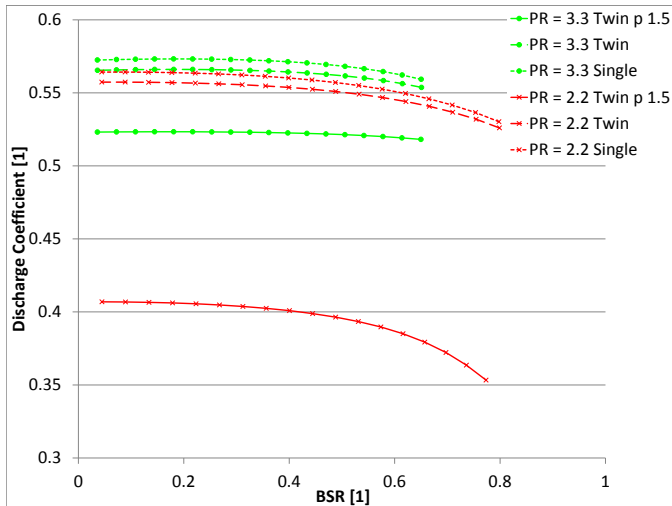


Figure 3. Total averaged discharge coefficient for a small turbine in dependence on blade speed ratio, rack position zero (closed vanes) with fixed pressure (mass-flow rate of 0.02 – 0.1 kg/s) and different distribution of pressure between entries (pressure difference 1.5 bar adjusted to the same mean pressure as in the case of full admission) compared to a single scroll case.

The results are nearly identical for both single scroll and twin scroll models in the case of uniform gas admission to both partitions, which was used as an initial test case of consistence of original single scroll and newly developed twin scroll model. This consistence check is very important because both GT Power models are completely different. E.g., twin scroll model uses momentum mixing modules not used in a single scroll model, which caused mentioned small differences.

The changes of turbine total discharge coefficient and turbine isentropic efficiency in case with non-uniform admission are clearly visible at different pressure ratios in presented example. Moreover, at low pressure difference between partitions neither discharge coefficient nor the efficiency is significantly reduced, since turbine achieves higher pressure in better supplied partition, which is of advantage for low rack position. After the pressure difference goes up to 1.5 bar, the differences change the trend in expected way, as demonstrated for efficiency in Figure 4.

The averaging of pressure ratio and ideal expansion isentropic velocity is subjected to imperfections due to compromised definitions in eq. (14)-(16), especially for a mass flow rates. That was why SAE maps are also introduced here. They feature the same trends, as presented for another (larger) turbine in Figure 5 and Figure 6. The efficiency totally changed the trend in dependence on pressure ratio due to changed turbine reaction. With the same dimensions of exducer, the impeller is relatively large if one of scroll partitions is almost closed. The trend is confirmed by experiments in [39]. If an exducer is too small for full admission, the efficiency at partial admission may even exceed efficiency for full admission if pressure ratio is high enough – see [39]. That is why the prediction from physically based model is so meaningful.

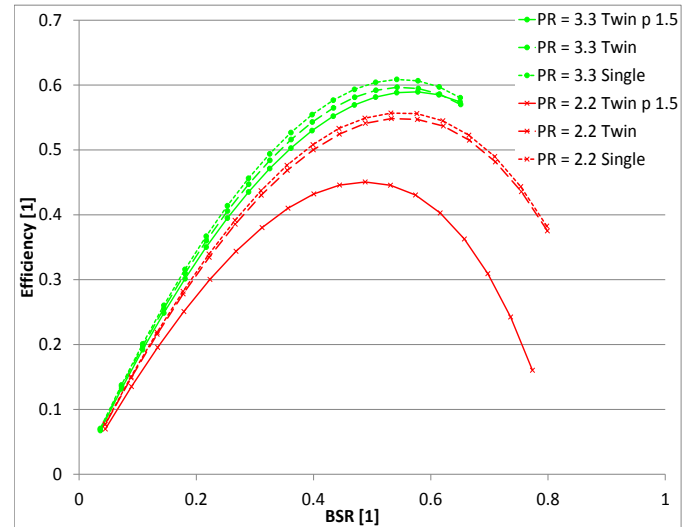


Figure 4. Isentropic efficiency for a small turbine in dependence on blade speed ratio, rack position zero (closed vanes) with fixed pressure (mass-flow rate of 0.02 – 0.1 kg/s) and different distribution of pressure between entries.

In both cases, total averaged maps were presented. There is no problem to calculate maps of this type for separated scroll partitions. Then, no questions about relevance of pressure ratio or ideal expansion velocity occur. This approach was used for a “0-D” map simulation described in the following chapter.

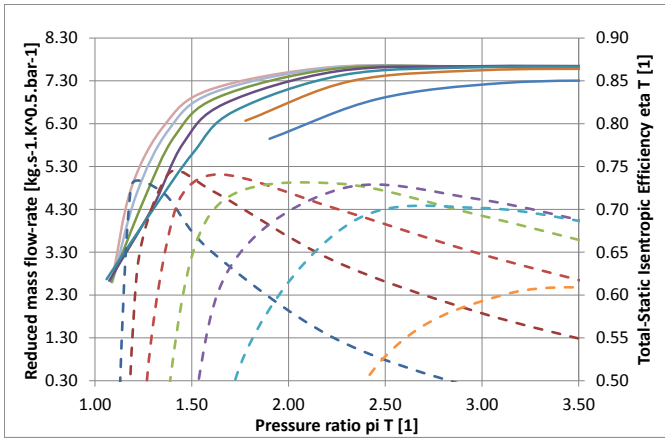


Figure 5. SAE Map – reduced mass flow-rate and isentropic efficiency for a larger turbine at equal distribution of flow between entries.

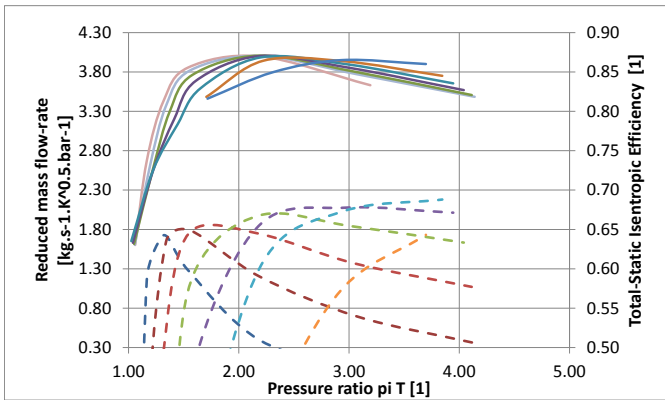


Figure 6. SAE Map – reduced mass flow-rate and isentropic efficiency for a larger turbine at fixed flow of 0.01 kg/s in one entry, variable flow from 0.05 till 0.5 kg/s in the other one.

Simulation of Engine with a Twin-Scroll Turbine

A four-cylinder turbocharged engine with the main data according to Table 1 was simulated at a speed of 2 000 r.p.m. with two different exhaust manifolds and two approaches to a turbocharger turbine specification.

Table 1. Basic parameters of a simulated engine.

Displaced volume	3054 cc
Bore	90 mm
Stroke	120 mm
Number of cylinders	4
Ignition order	1-3-4-2
Single scroll manifold volume	1.1 dm ³
Twin scroll partition A cyls. 1+4	0.8 dm ³
Twin scroll partition B cyls. 3+2	0.5 dm ³

The first manifold was a simple symmetric single-pipe, all-cylinders connecting to collector of 1.1 dm³ volume for a single scroll lay-out. The other one was an asymmetrical two-pipe, twin-scroll manifold with branches described in Table 1 and presented as a GT Power model in Figure 23.

To find the features of newly developed model, comparison of different modelling approaches to a twin-scroll turbine was done. The full 1-D model for both branches and partitions was compared to a lumped-parameter 0-D model, based on a virtual test bed results at equal admission to both scroll partitions. Turbine was divided into two sections with a half flow-rate capacity. The model was calibrated to reach the same A/F ratio with both approaches.

The simulations were done for several operation modes at high load of approximately 12 bar of bmep at 2 000 r.p.m., high A/F ratio (relative A/F of 2, closed rack position) with bsfc of 244 g/kW/h and turbine inlet temperature of 800 K, high load – high rack position mode with relative A/F of only 1.75, bmep of 9.5 bar approximately, bsfc of 230 g/kW/h and the same turbine inlet temperature and finally for low load, high A/F (relative A/F approx. 4.5, closed rack position), bsfc 435 g/kW/h and turbine inlet temperature of approx. 565 K only.

Twin scroll with this standard 0-D map approach for a half of a turbine does not respect any influence of the joint manifold branch. The mass flow rates in Figure 7 - Figure 8 reflect this feature by higher mass flow rate, especially just before the next branch pressure wave comes. On the other hand, deeper pressure decrease at the end of exhaust pulse is featured by this 0-D approach - Figure 9 - Figure 11. It is obvious that those phenomena work against each other. Therefore, the physics of 0-D model is not realistic. The difference in pressures and mass flow rates leads to different turbine power and consequently to different turbocharger speed, as demonstrated in Figure 14 - Figure 16 and in Figure 13.

0-D model can be empirically repaired by adding a throttled cross-link between both manifolds upstream of a turbine, as recommended by Gamma Technologies – [28] and used in [39]. The throttle area has to be changed for different operation conditions, however, because the connection of flows is done, in reality, at non-existing pressure difference.

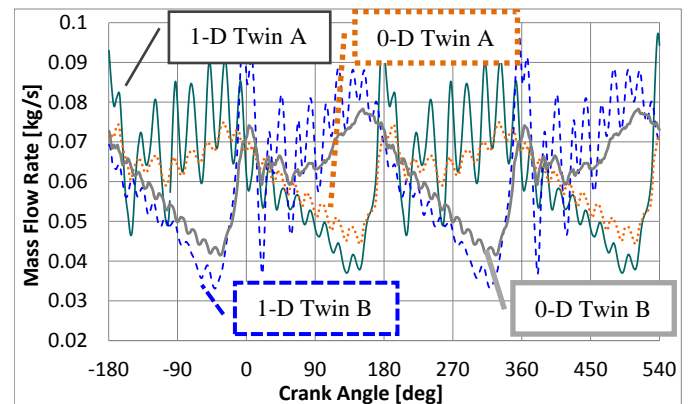


Figure 7. Mass flow rate in both partitions of a twin scroll using different turbine models. Bmep approx. 12 bar, 2 000 r.p.m., boost pressure approx. 2.8 bar.

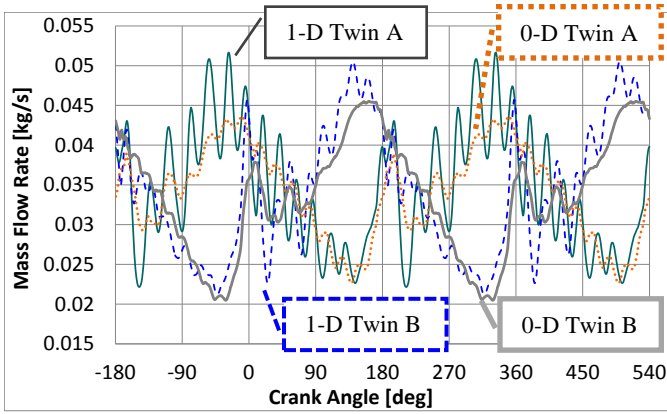


Figure 8. Mass flow rate in both partitions of a twin scroll using different turbine models. Bmep approx. 1.8 bar, 2 000 r.p.m., boost pressure approx. 1.4 bar. See Figure 11.

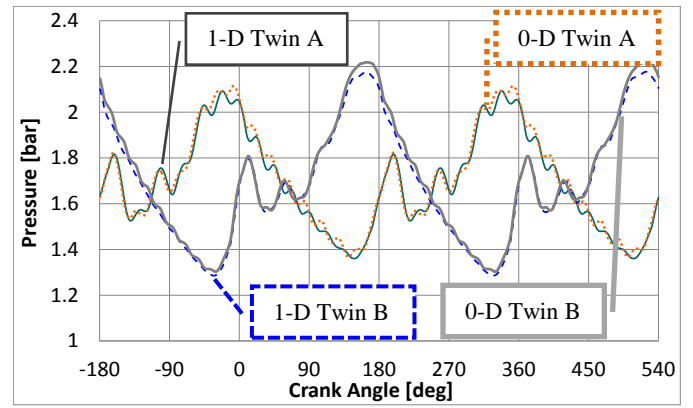


Figure 11. Pressures at turbine entries for both twin-scroll turbine entries A and B for different models (1-D and lumped parameters 0-D) and bmep approx. 1.8 bar, 2 000 r.p.m., boost pressure approx. 1.4 bar.

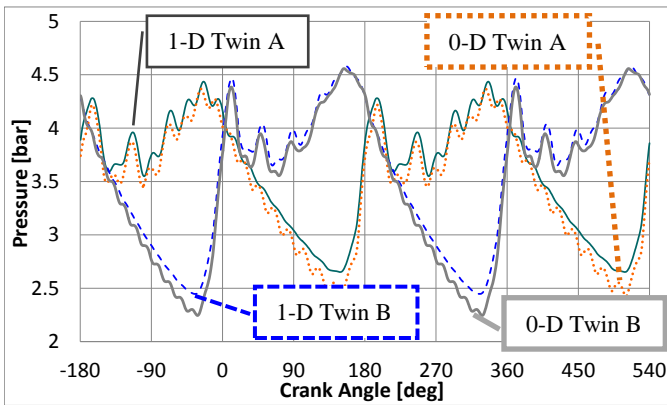


Figure 9. Pressures at both twin-scroll turbine entries A and B for different models (1-D and lumped parameters 0-D) and bmep approx. 12 bar, 2 000 r.p.m., boost pressure approx. 2.8 bar.

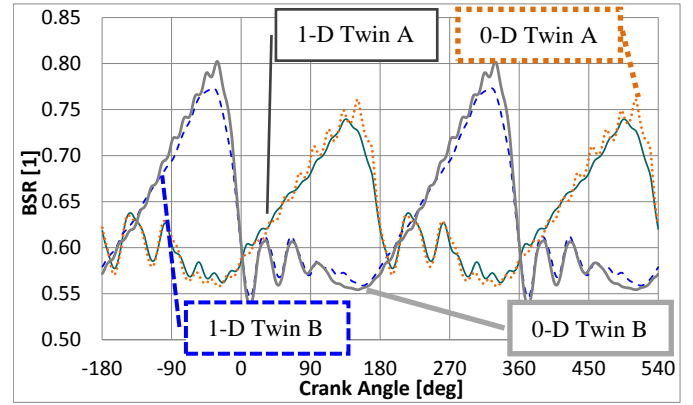


Figure 12. Blade speed ratio for both turbine scroll partitions at bmep approx. 12 bar, 2 000 r.p.m., boost pressure approx. 2.8 bar in dependence on turbine model.

The mass flow rate would be still too high in this case using realistic turbine flow area found by steady-flow experiments, since the counter-acting influence of the pressure pulse from the other manifold does not exist in this model. That is why the turbine test bed results have to be calibrated by experiments at an engine.

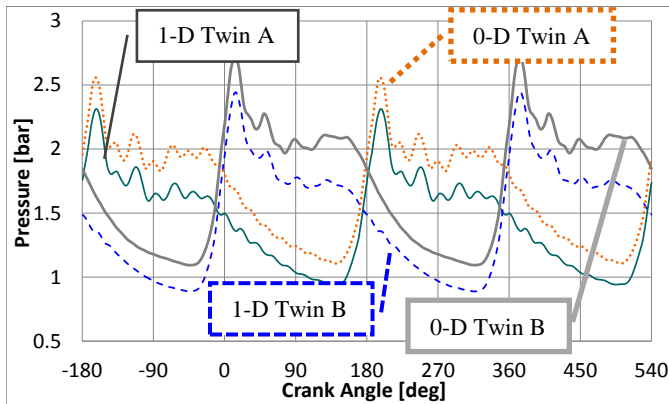


Figure 10. Pressures at both twin-scroll turbine entries A and B for different models (1-D and lumped parameters 0-D) and bmep approx. 9.5 bar, 2 000 r.p.m., boost pressure approx. 1.65 bar.

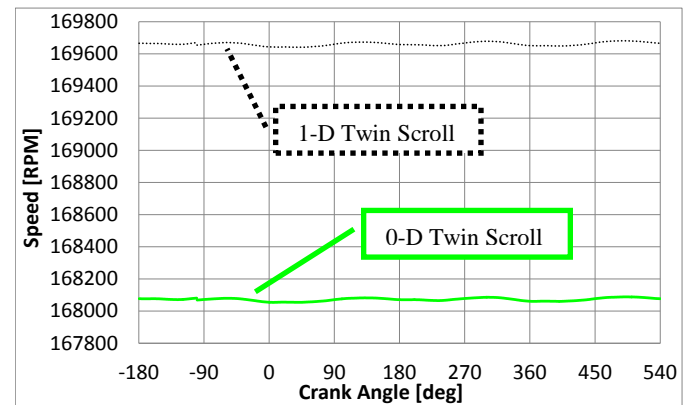


Figure 13. Predicted turbocharger speed in dependence on turbine model. Bmep approx. 12 bar, 2 000 r.p.m., boost pressure approx. 2.8 bar.

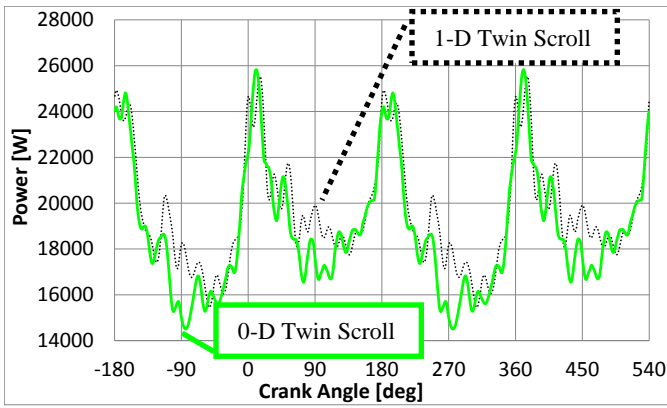


Figure 14. Turbine shaft power in dependence on the model type at high engine load, high A/F ratio. Bmep approx. 12 bar, 2 000 r.p.m., boost pressure approx. 2.8 bar.

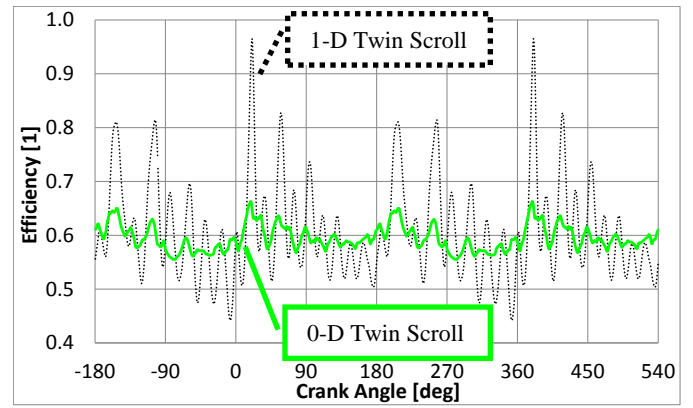


Figure 17. Turbine isentropic efficiency evaluated for state at both sides of a turbine in dependence on the model type. Bmep approx. 12 bar, 2 000 r.p.m., boost pressure approx. 2.8 bar.

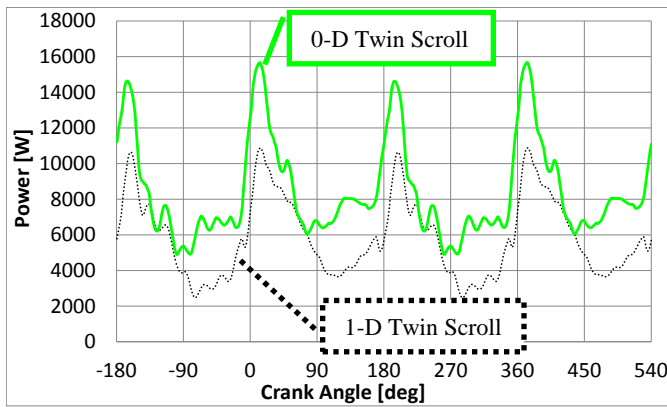


Figure 15. Turbine shaft power in dependence on the model type. Bmep approx. 9.5 bar, 2 000 r.p.m., boost pressure approx. 1.65 bar.

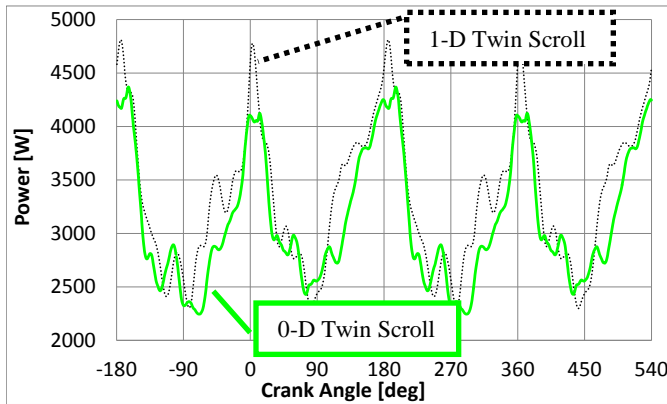


Figure 16. Turbine shaft power in dependence on the model type at low engine load, high A/F ratio (rack position close to zero). Bmep approx. 1.8 bar, 2 000 r.p.m., boost pressure approx. 1.4 bar.

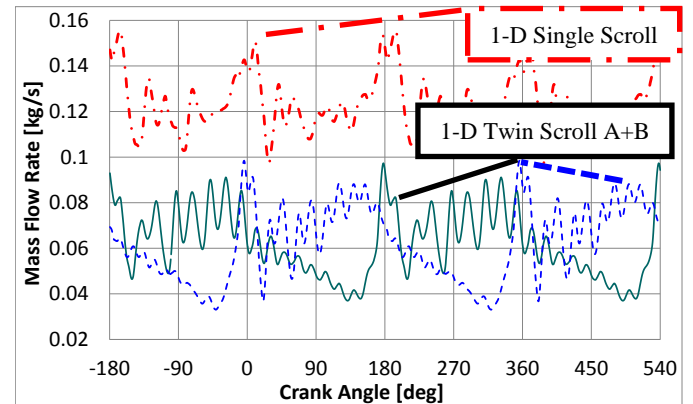


Figure 18. Mass flow rate in both partitions of a twin scroll and in a single scroll turbine. Bmep approx. 12 bar, 2 000 r.p.m., boost pressure 2.8 bar.

The investigated features of a full 1-D model are currently being subjected to testing at an experimental six cylinder engine and at a specific facility with divided inlets to a twin scroll turbine. The qualitative analysis of the results has allowed finding interesting differences, significantly supporting the philosophy of a full 1-D. The necessary extrapolations of turbine maps can be done quite naturally, no additional artificial modifications of the engine model are needed.

The full 1-D model may be important for appropriate prediction of initial conditions for a transient load acceptance. The natural extrapolation of parameters seems to be worthwhile for those practically important cases, in which the differences between real and simulated boost pressures are not important (pressures being close to atmospheric ones in any case) but the starting turbocharger speed influences the transient response significantly.

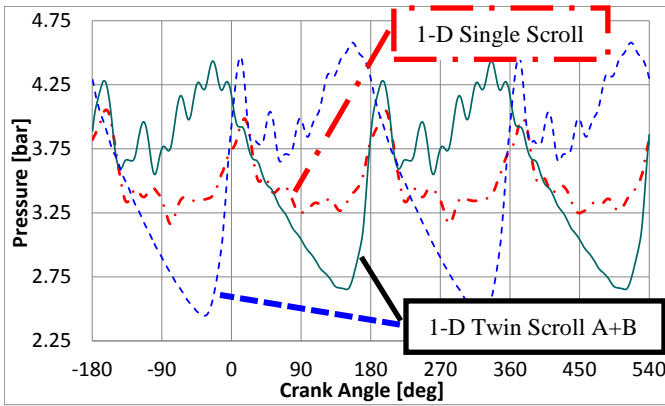


Figure 19. Pressures at inlets to both partitions of a twin scroll turbine and at a single scroll turbine. Bmep approx. 12 bar, 2 000 r.p.m., boost pressure approx. 2.8 bar.

After those introductory tests, the model was used for comparison of a single and twin scroll layouts of turbine at a four cylinder engine. Selected examples are in Figure 18 - Figure 21 for mass flow rate, pressures upstream a turbine, BSR and turbine power. The presented cases for high load, closed rack position are qualitatively the same if load or rack position is changed.

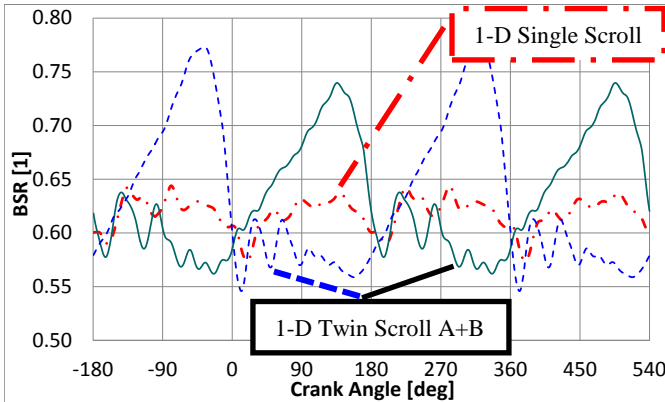


Figure 20. Blade speed ratio for both turbine twin scroll partitions and for a single scroll turbine at high load: bmep approx. 12 bar, 2 000 r.p.m., boost pressure approx. 2.8 bar in dependence on turbine model.

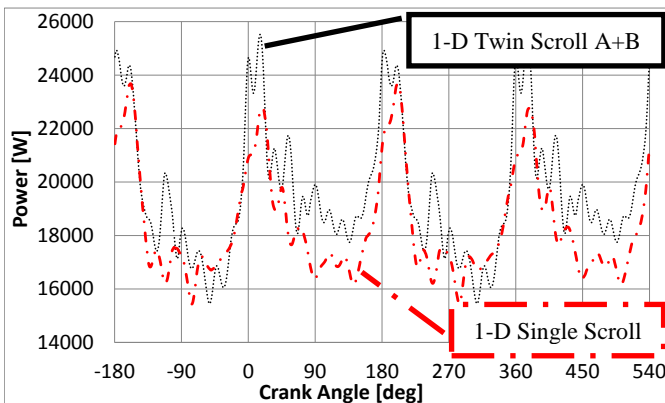


Figure 21. Turbine power for a twin scroll turbine and a single scroll turbine. High load. Bmep approx. 12 bar, 2 000 r.p.m., boost pressure approx. 2.8 bar

The results confirm the well-known feature of pulse exhaust system and twin scroll turbine. The power transferred from a cylinder is much higher in branches connected to a twin scroll, which is obvious from Figure 21.

At the other side, the pumping work is increased, as well, which influences bsfc especially while closing rack position. In the case of 12 bar of bmeP at 2 000 r.p.m., high A/F ratio (relative A/F of 2, closed rack position) bsfc was increased from 234 to 244 g/kW/h switching from a single scroll to twin one. Opening a turbine for high rack position with relative A/F of only 1.75 and bmeP of 9.5 bar approximately, bsfc was increased only moderately from 230 to 232 g/kW/h. Finally, for low load, high A/F (relative A/F approx. 4.5, closed rack position), bsfc was changed from single scroll 400 g/kW/h to nearly 430 g/kW/h using twin scroll lay-out.

Those preliminary results will be generalized to other engine speeds and configurations of exhaust manifold and compared to dedicated experiments in a near future. The results have been already achieved but they are still confidential.

Procedure of Model Calibration

As described above, both algebraic central streamline quasi-steady model and full physically based model with wave phenomena inside all parts of turbine have been developed. Both models were tested in 1-D solver, aiming at replacing the necessity to interpolate in turbine maps for different partial admission and taking into account the real unsteadiness of turbine flow in the latter case. Nevertheless, the models are not fully predictive if not calibrated before use.

The procedure, tested up to now for the case of single scroll model is based on the following steps:

- testing of a turbine at real, steady flow test bed with different level of partial admission;
- simulation of virtual turbine maps for different partial admission cases using quasi steady or unsteady physical model at virtual turbine test bed at the same operating conditions as above;
- optimizing the turbine model tuning parameters by genetic algorithm, as described for a single scroll model in [24] and [26]; assessment of errors by comparing virtual turbine maps and measured real turbine maps;
- direct use of calibrated models in 1-D simulation, using all features of complete unsteady engine model; the model replaces in this case standard maps of a turbine, yielding directly the turbine mass flow rate and power in dependence on pressures and inlet temperatures in turbine environment.

Summary/Conclusions

A model of a twin scroll turbine using central streamline 1-D approach has been developed for both steady and unsteady partial admission flows. The model is currently available for parallel scroll partitions but its layout makes it possible to extend it to serial scrolls just by changing mixing location of both scroll flows.

The newly developed really physically based twin scroll turbine model has been tested on a four cylinder engine model with single and twin exhaust manifolds from the point of view of reliability and extrapolation capacity. The numerical features and qualitative predictive capabilities are satisfactory. The model needs some additional modifications, e.g., taking reversed flows at very low admission ratios into account. Nevertheless, even the current state of the model is sufficient for its practical implementation up to high, supercritical pressure ratios.

The model has been tested by dedicated experiments but the results are still confidential. The qualitative comparison can be published only at this time. Experiments have been recently carried out on a six cylinder, twin manifold engine. A specific test bed with distributed flows to a twin scroll turbocharger is already prepared.

The implementation into 1-D commercial codes, e.g., GT Power can be done for both models without significant problems. It can create an efficient tool for optimization of downsized highly dynamic engines, based on physics of unsteady flow and thus insensitive to changes of a current engine layout.

A comparison of the presented turbine model with a map based quasi- steady turbine is being prepared for further studies.

References

1. Zinner, K., "Supercharging of Internal Combustion Engines". Springer Heidelberg 1978
2. Shapiro, A. H., "The Dynamics and Thermodynamics of Compressible Fluid Flow," The Ronald Press Comp., New York 1953.
3. Jenny, E., "Berechnungen und Modellversuche über Druckwellen grosser Amplituden in Auspuff-Leitungen," Dissertation ETH Zürich, Ameba Druck Basel 1949.
4. Watson, N., Janota, M.S., "Turbocharging the Internal Combustion Engine". MacMillan Publishers, London 1982, ISBN 0 333 24290 4
5. Sherstjuk, A. N., Zarjankin A. E.: Radial-Axial Turbines of a Small Power (in Russian). Mashinostroenije, Moscow 1976
6. Dibelius G.: Partial Admission of Turbocharger Turbines (in German). Brown Boveri Mitteilungen Vol. 52, 1965, 3
7. Bulaty T.: Specific Problems of 1-D Models of Gas Exchange at Turbocharged Engines (in German). Motortechnische Zeitschrift Vol. 35, 1976, 4
8. Winterbone, D.E. et al., "A Contribution to the Understanding of Turbocharger Turbine Performance in Pulsating Flow". Int. Conf. on Internal Engine Research, Paper C433/011, Instn.Mech.Engrs. London 1991
9. Hu, Xiao, Lawless, P.B., "Predictions of On-Engine Efficiency for the Radial Turbine of a Pulse Turbocharged Engine". SAE Paper 2001-01-1238
10. Lujan, J.M., Galindo, J., Serrano, J.R., "Efficiency Characterization of Centripetal Turbines under Pulsating Flow Conditions". SAE Paper 2001-01-0272
11. Dunham, J., Came, P.: Improvements to the Ainley-Mathieson Method of Turbine Performance Prediction. Trans. ASME, Series A, Vol. 92, 1970
12. Capobianco, M., Marelli, S., "Turbocharger Turbine Performance Under Steady and Unsteady Flow: Test Bed Analysis and Correlation Criteria". 8th Intl. Conf. on Turbochargers and Turbocharging, IMechE London, 2006
13. Capobianco, M., Marelli, S., "Unsteady Flow Behaviour of the Turbocharging Circuit in Downsized Automotive Engines". FISITA Congress 2006, Yokohama, paper F2006P119, 12 pp.
14. Capobianco, M., Marelli, S., "Transient Performance of Automotive Turbochargers: Test Facility and Preliminary Experimental Analysis". SAE Paper 2005-24-66
15. Capobianco, M., Gambarotta, A., "Variable Geometry and Waste-Gated Automotive Turbochargers: Measurements and Comparison of Turbine Performance". Journal of Engineering for gas Turbines and Power, Volume 114, 1992, pp. 553-560
16. Gurney, D., "The Design of Turbocharged Engines Using 1-D Simulation". SAE Paper 2001-01-0576
17. Winkler, N., Angstrom, H.E., Olofsson, U., "Instantaneous On-Engine Twin-Entry Turbine Efficiency Calculations on a Diesel Engine". SAE Paper 2005-01-3887
18. Winkler, N., Angstrom, H.E., Olofsson, U., "Instantaneous On-Engine Turbine Efficiency for a SI Engine in the Closed Waste Gate Region for 2 Different Turbochargers". SAE Paper 2006-01-3389
19. Westin, F., Angstrom, H.E., "Calculation Accuracy of Pulsating Flow through the Turbine of SI-Engine Turbochargers". SAE Paper 2005-01-0222
20. Osako, K., Higashimori, H., Mikogami, T., "Study on the Internal Flow of Radial Turbine Rotating Blades for Automotive Turbochargers". SAE Paper 2002-01-0856
21. Costall, A., Szymko, S., Martinez-Botas, R.F., Filsinger, D., Ninkovic, D., "Assessment of Unsteady Behaviour in Turbocharger Turbines". Proceedings of ASME TurboExpo 2006, pap. GT2006-90348, Barcelona 2006
22. Serrano, J., Arnau, F., Novella, R., and Reyes-Belmonte, M., "A Procedure to Achieve 1D Predictive Modeling of Turbochargers under Hot and Pulsating Flow Conditions at the Turbine Inlet". SAE Technical Paper 2014-01-1080, 2014, doi:10.4271/2014-01-1080.
23. Macek, J. - Vávra, J. - Vitek, O., "1-D Model of Radial Turbocharger Calibrated by Experiments". SAE Paper 2002-01-0377. In: Modeling of SI Engines and Multi-Dimensional Engine Modeling. Warrendale, PA : Society of Automotive Engineers, 2002, vol. 1, p. 173-194. ISBN 0-7680-0970-7.

24. Macek J., Vítek O., Žák Z., Vávra J., “Calibration and Results of a Radial Turbine 1-D Model with Distributed Parameters”. SAE Paper 2011-01-1146, 30 pp.
25. Macek J., Vítek O., Burič J. and Doleček V., “Comparison of Lumped and Unsteady 1-D Models for Simulation of a Radial Turbine”. SAE Int. J. Engines Vol.2(1) 173-188, 2009, ISSN 1946-396. SAE Paper 2009-01-0303
26. Macek, J., Vítek, O., “Simulation of Pulsating Flow Unsteady Operation of a Turbocharger Radial Turbine”. SAE Paper 2008-01-0295, 20 pp.
27. Vávra J., Macek J., Vítek O., Takáts M., “Investigation of Radial Turbocharger Turbine Characteristics under Real Conditions”. Modeling of SI and CI Engines. SAE SP-2244, ISBN 978-0-7680-2140-0, 2009, (SAE Paper.2009-01-0311).
28. GT-POWER, USER’S MANUAL and Tutorial GT-Suite™ version 7.4, Private Publication Gamma Technologies Inc., Westmont IL, 2013
29. T. Morel, R. Keribar and A. Leonard, “Virtual Engine/Powertrain/Vehicle Simulation Tool Solves Complex Interacting System Issues”, SAE Paper 2003-01-0372
30. Bogomolov S., Macek J. and Mikulec A., “Development of Design Assistance System and Its Application for Engine Concept Modeling”. SAE Paper 2011-37-0030. 11 pp.
31. Vítek, O., Macek, J., Polášek, M., “New Approach to Turbocharger Optimization using 1-D Simulation Tools”. SAE Paper 2006-01-0438, SAE Int. Warrendale 2006, 15 pp.
32. Pohořelský, L., Žák, Z., Macek, J., Vítek, O., “Study of Pressure Wave Supercharger Potential using a 1-D and 0-D Approach,” SAE Paper 2011-01-1143, 2011
33. Brynych P., Macek J., Vítek O., Cervenka L.: 1-D Model of Roots Type Supercharger. SAE 2013-01-0927. Engine Boosting Systems, 2013. SAE COLL-TP 00363, pp. 14 ISSN 0148-7191
34. N. Brinkert, S. Sumser, A. Schulz, S. Weber, K. Fieweger and H.-J. Bauer. Understanding the twin-scroll turbine-flow similarity. ASME Turbo Expo, GT2011-46820, 49:2207–2218, 2011.
35. De Bellis, V., Bozza, F., Schernus, C., and Uhlmann, T., Advanced Numerical and Experimental Techniques for the Extension of a Turbine Mapping, SAE Int. J. Engines 6(3):2013, doi:10.4271/2013-24-0119
36. C. F. Fredriksson, Xuwen Qiu, N. C. Baines, M. Müller, N. Brinkert and C. Gutmann. Meanline Modeling of Radial Inflow Turbine With Twin-Entry Scroll. ASME Turbo Expo 2012, doi:10.1115/GT2012-69018
37. R. Aymanns; J. Scharf; T. Uhlmann; S. Pischinger. Turbocharger Efficiencies in Pulsating Exhaust Gas Flow. MTZ, vol. 07-08/2012.
38. D. Lückmann; T. Uhlmann; H. Kindl; S. Pischinger. Separation in Double Entry Turbine Housings at Boosted Gasoline Engines. MTZ, vol. 10/2013
39. Uhlmann, T., et al. Development and Matching of Double Entry Turbines for the Next Generation of Highly Boosted Gasoline Engines. 34th International Vienna Motor Symposium. 2013.
40. Mikula, M.: Modelling and Optimization of Pulse Converters for Highly Turbocharged Medium Speed Engines (in Czech). PhD Thesis, Czech Technical University 1985
41. Macek, J., Mikula, M.: Optimization of Exhaust Systems for Turbocharged Diesel Engines (in Czech). Technical Contributions of CKD PRAHA Heavy Industries, 18, 1985, pp. 11-28, ISSN 0322-8523

Contact Information

Jan.Macek@fs.cvut.cz

Acknowledgments

This work was supported by:

- Technological Agency, Czech Republic, programme Centre of Competence, project #TE01020020 Josef Božek Competence Centre for Automotive Industry.
- EU Regional Development Fund in OP R&D for Innovations (OP VaVpI) and Ministry of Education, Czech Republic, project #CZ.1.05/2.1.00/03.0125 Acquisition of Technology for Vehicle Center of Sustainable Mobility.
- Zvoníček’s Foundation, Czech Republic, project - Development of a 1-D Model of a Radial Turbocharger Turbine Supported by the Financial Donation of Dr. Thomas Morel

This support is gratefully acknowledged.

Definitions/Abbreviations

SYMBOLS

A	flow area [m ²]
a	velocity of sound [m.s ⁻¹]
b	vane axial width [m]
C	correction to compressibility [1]
c	absolute velocity [m.s ⁻¹]
c_p	isobaric specific heat capacity [J.kg ⁻¹ .K ⁻¹]
c_s	velocity after isentropic expansion of a total enthalpy head, ideal expansion velocity [m.s ⁻¹]
D	diameter [m]
h	specific enthalpy [J.kg ⁻¹]
K	tuning coefficient [1]
M	torque [N.m]
m	mass, mass flow rate (with dot) [kg, kg.s ⁻¹]
n	speed [min ⁻¹]
P	power [W]
p	pressure [Pa]
Re	Reynolds number [1]
r	specific gas constant [J.kg ⁻¹ .K ⁻¹]
r	radius [m]
s	specific entropy [J.kg ⁻¹ .K ⁻¹]
T	temperature [K]
u	circumferential velocity [m.s ⁻¹]
w	relative velocity [m.s ⁻¹]
x	blade tip velocity ratio u_2/c_s [1]
z	number of blades [1]
α	angle of absolute velocity (measured from radial or axial direction) [deg]
β	angle of relative velocity (measured from radial or axial direction) [deg]
ε	pressure ratio <1 [1]
η	isentropic efficiency [1]
ζ	kinetic energy loss coefficient [1]
κ	isentropic exponent [1]
λ	power input coefficient [1]
μ	discharge coefficient
ν	kinematic viscosity [m ² .s ⁻¹]
π	pressure ratio >1 [1]
ρ	density [kg.m ⁻³]
τ	shear stress [Pa]
ψ	flow function [1]
ω	angular velocity [rad.s ⁻¹]

SUBSCRIPTS

a	axial
app	approximation
comp	compressible
F	friction

I	impeller
inc	incidence, angle of attack
incomp	incompressible
K	compressor
leak	leakage
N	nozzle ring, vaneless turbine scroll&nozzle
nom:	nominal, at maximum efficiency
r	radial
red	reduced
rel	relative flow
s	isentropic
sep	flow separation
vent	windage
T	turbine
t	tangential
vl	vaneless
0	total or stagnation state
1	inlet
2	outlet or nozzle ring outlet
3	impeller outlet
‘	blade root
“	blade tip

ACRONYMS

bmeP	brake mean effective pressure
bsfc	brake specific fuel consumption
BSR	blade speed ratio u/c_s
CR	centripetal radial
CRT	centripetal radial turbine
ICE	internal combustion engine
VG	variable geometry
VGt	variable geometry turbine
WG	waste-gate

Appendix

The Appendix is one-column. If you have an appendix in your document, you will need to insert a continuous page break and set the columns to one. If you do not have an appendix in your document, this paragraph can be ignored and the heading and section break deleted.

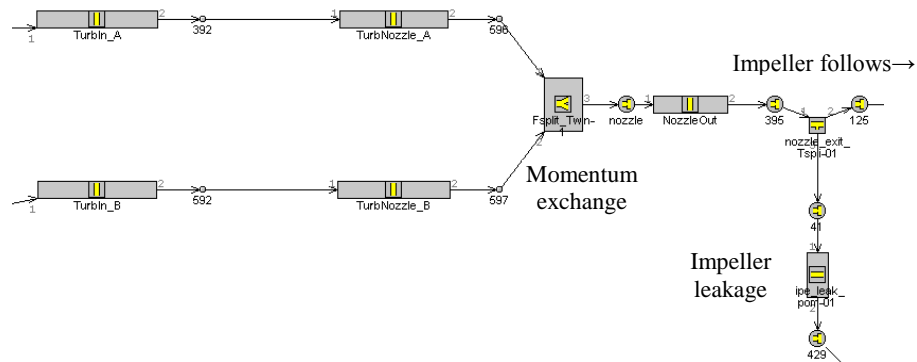


Figure 22. Simplified model of a GT Power inlet scroll model for an unsteady flow inside a scroll and mixing of both flows after partial expansion.

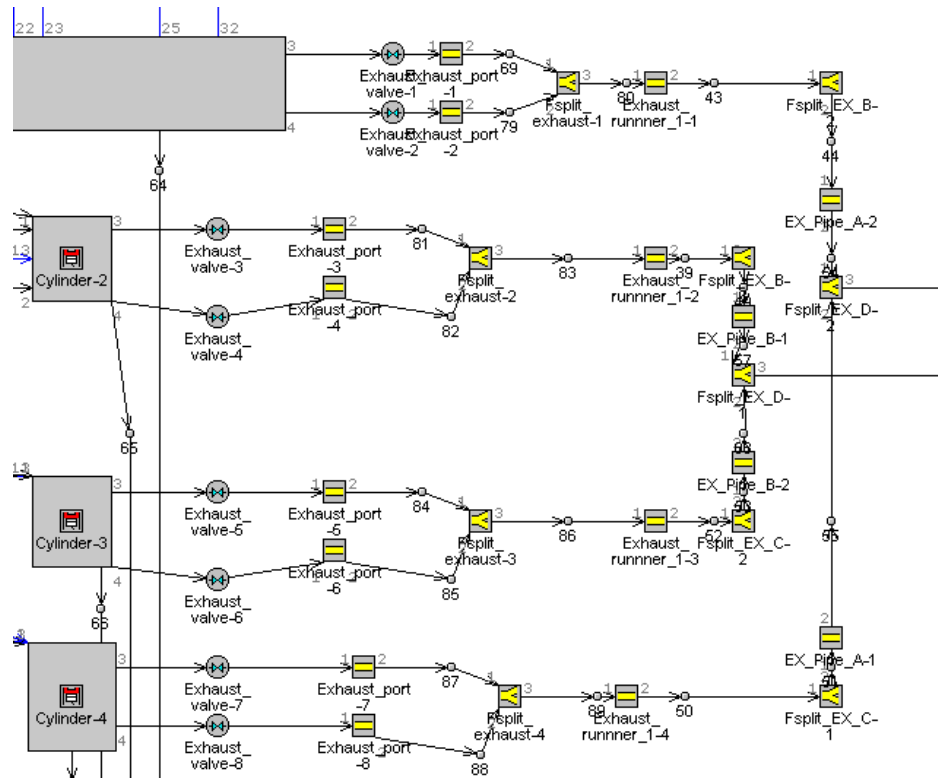


Figure 23. The scheme of a four-cylinder engine model with pulse exhaust manifold consisting of two partitions (ignition order 1-3-4-2) coupled to a twin entries according to Figure 22.